

Generation of continuous-variable cluster states of cylindrically polarized modes

Ioannes Rigas,^{1,2,*} Christian Gabriel,^{1,2,*} Stefan Berg-Johansen,^{1,2} Andrea Aiello,^{1,2}
Peter van Loock,^{1,2,3} Ulrik L. Andersen,^{1,2,4} Christoph Marquardt,^{1,2} and Gerd Leuchs^{1,2}

¹Max Planck Institute for the Science of Light, Staudtstr. 2, D-91058 Erlangen, Germany

²Institute of Optics, Information and Photonics, University Erlangen-Nuremberg, Staudtstr. 7/B2, D-91058 Erlangen, Germany

³Institute of Physics, University of Mainz, Staudingerweg 7, 55128 Mainz, Germany

⁴Department of Physics, Technical University of Denmark, 2800 Kongens Lyngby, Denmark

Cluster states are an essential component in one-way quantum computation protocols. We present two schemes to generate addressable continuous-variable cluster states from quadrature squeezed cylindrically polarized modes. By including polarization in addition to the transverse spatial degree of freedom, elementary cluster states can be created in which four cluster nodes co-propagate within one paraxial vector beam. This approach is fundamentally compatible with existing time-multiplexed schemes that have been used to create the largest cluster states to date. We implement a proof-of-principle experiment of one of the proposed schemes and verify its feasibility by measuring the quantum correlations between the different nodes of the cluster state.

PACS numbers: 03.67.Lx, 42.50.Dv, 03.65.Ud, 03.67.Bg

The efficient processing of computational tasks is extremely desirable in today's fast-evolving information society. Quantum computers have the potential to clearly outperform classical systems at certain computational operations [1]. While recent years have seen a steady development in the technologies necessary for full-scale quantum computing, work continues also on foundational concepts and new implementation candidates. It has been shown that so-called cluster states represent a universal resource for measurement-based, one-way quantum computation, which can be performed with discrete-variable (DV) systems [2–6] as well as with continuous-variable (CV) quantum states [7–18]. In these schemes specially prepared entangled states, the cluster states, form the backbone of the protocol. The central idea behind cluster-state quantum computation is to enact quantum logic gates on parts of an initially prepared cluster state by teleporting them through the cluster. These gates are then implemented solely by means of local measurements, while additional Hadamard (DV) or Fourier (CV) gates are built-in along the teleportations to switch between different bases and obtain universality. The first measurement results determine which bases to choose for the remaining measurements and which Pauli (DV) or displacement (CV) corrections to apply. Thus, in this model, the complication of implementing deterministic quantum gates is transferred to the task of generating highly non-locally correlated cluster states, typically, either in a probabilistic (DV) or deterministic (CV) fashion [19].

There has been significant progress in generating large scale CV cluster states in recent years. The first realization of CV cluster states relied on the generation of individually squeezed states from different optical parametric oscillators supporting the same Gaussian spatial modes. The modes interfere in a linear network of beam splitters to create a cluster state of four modes [9, 20]. This idea was then extended to higher order spatial modes combined with a programmable spatial mode detector rendering the system much more compact [21]. These methods did not allow for large scale cluster states to be formed. However, excellent scalability can

be attained by making use of the inherent quantum correlations between frequency modes of an optical parametric oscillator [10, 12, 13, 22] or by using the temporal-mode quantum correlations [23, 24]. Using these two approaches, cluster states of 16 modes [17], 60 modes [25] and 10^6 modes [26, 27] have been generated, respectively.

Here, we report on new schemes to generate a four-state cluster with the help of quadrature squeezed cylindrically polarized modes. These modes have a nonseparable structure leading to useful properties both in a quantum [28] and classical optics setting [29]. The resulting cluster states rely on the four orthogonal bases of the cylindrically polarized modes which can be easily distinguished and addressed. This approach to cluster generation is related to the approach of Ref. [21] where the different eigenmodes of the cluster correspond to the higher-order Hermite-Gaussian spatial modes. However, in our proposal, we add the polarization as another degree of freedom, thereby extending the mode space by a factor of two and promoting the flexibility in addressing the various modes. The approach can be extraordinarily compact as all involved modes can be generated in a single optical parametric oscillator using the process of parametric downconversion [30, 31] or by using the optical Kerr effect of an optical fiber [28, 32]. The schemes we propose here are designed in such a way that they offer, at the same time, a compact and robust cluster-state preparation as well as an easy and direct addressability of the nodes of the cluster. At the end of this paper, we report on a proof-of-principle demonstration of one of the proposed schemes, for which we measure the quantum correlations present among all the four nodes of the cluster state.

For continuous variables, in the limit of infinite squeezing, cluster states fulfill the eigenequation [11]

$$\left(\hat{p}_j - \sum_{k \in N_j} A_{jk} \hat{q}_k\right) |\psi\rangle \rightarrow 0 \quad \forall j. \quad (1)$$

This is in analogy to the discrete case, where cluster states are eigenstates of the Pauli stabilizers $\hat{\sigma}_x^{(j)} \prod_{k \in N_j} \hat{\sigma}_z^{(k)}$ [33]. In

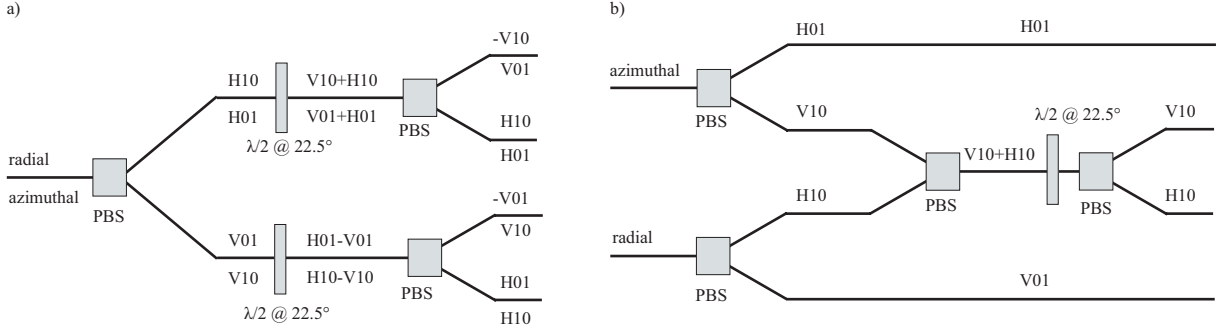


FIG. 1: a) Scheme 1 for cluster-state generation. A radially polarized mode enters a linear-optics network with the four output modes then forming a cluster state. The radially polarized mode could also be substituted by an azimuthally polarized one to generate a similar cluster state. b) Scheme 2 for cluster-state generation. One radially and one azimuthally polarized mode form the input state. The four output modes again constitute a cluster state. [polarizing beam splitter (PBS), half-wave plate ($\lambda/2$)].

the CV case, \hat{p}_j and \hat{q}_j correspond to the “position” and “momentum” operators of the optical mode j . N_j are the adjacent modes of the mode j . The real matrix \mathbf{A} contains the full information about the cluster or, equivalently, its graph. It therefore determines what the displacement corrections after measuring some of the modes must be in order to achieve, in principle, unit-fidelity teleportation. This is reflected by the fact that the covariances of the operators ($\hat{p}_j - \sum_k A_{jk} \hat{q}_k$), which correspond to the excess noises acquired during the individual teleportation steps, all vanish. Note that in a two-mode scenario, the state that satisfies Eq. (1) is the famous EPR state up to a local Fourier rotation.

In any realistic scenario, however, one is limited to finitely squeezed input states. Thus, quantum teleportation using realistic cluster states always has non-unit fidelities, so that these physical clusters are non-ideal states for universal quantum computation. Nevertheless, one can define *approximate* cluster states or *Gaussian graph states* [14] which clearly specify the correlations between the individual modes in a cluster, as well as the infidelities of the quantum operations that have to be accepted for a finite degree of squeezing. The full information on any (zero-mean) Gaussian state is contained in its covariance matrix. CV cluster states can then be completely described by the adjacency matrices of their graphs [14], defined as,

$$\mathbf{Z} = i\mathbf{U} + \mathbf{V}. \quad (2)$$

Here, \mathbf{U} and \mathbf{V} are given by

$$\mathbf{U} = \frac{1}{2} \langle \hat{\mathbf{q}} \hat{\mathbf{q}}^T \rangle^{-1}, \quad \mathbf{V} = \langle \hat{\mathbf{q}} \hat{\mathbf{q}}^T \rangle^{-1} \times \langle \{ \hat{\mathbf{q}}, \hat{\mathbf{p}}^T \} \rangle, \quad (3)$$

where $\langle \hat{\mathbf{q}} \hat{\mathbf{q}}^T \rangle$ denotes the position covariance matrix and $\langle \{ \hat{\mathbf{q}}, \hat{\mathbf{p}}^T \} \rangle$ the matrix describing the cross-correlations between position and momentum, defined as $\langle \{ \hat{\mathbf{q}}, \hat{\mathbf{p}}^T \} \rangle_{jk} = \frac{1}{2} \langle (\hat{q}_j \hat{p}_k + \hat{p}_k \hat{q}_j) \rangle$. The role of \mathbf{U} is to incorporate the finite squeezing of each mode, while \mathbf{V} represents the coupling between the modes. For the complex adjacency matrix \mathbf{Z} , replacing the real matrix \mathbf{A} , Eq. (1) becomes an exact zero-eigenvalue equation even for finite squeezing [14]. It is therefore

a convenient tool to quantify and describe finitely squeezed cluster states.

For a realistic cluster with finite squeezing, the complex adjacency matrix now determines both the necessary displacements during teleportation and the excess noise that inevitably will be added to the state after teleportation: the covariances of the operators ($\hat{p}_j - \sum_k V_{jk} \hat{q}_k$) are given by the matrix elements $U_{nm}/2$, so that the total matrix \mathbf{Z} contains the full information on the intermode correlations of a cluster state.

Our cluster-state generation schemes are based on cylindrically polarized beams. These can be described by a superposition of two out of four distinct modes. If one chooses, for example, the Hermite-Gaussian basis to define cylindrically polarized modes, this would be the two first-order Hermite Gaussian TEM_{10} (10) and TEM_{01} (01) with horizontal (H) and vertical (V) polarization, namely $H10$, $V10$, $H01$ and $V01$ [34]. In Ref. [28] we have shown that by quadrature squeezing a cylindrically polarized beam, one generates squeezing in and entanglement between the basis modes. Our cluster states rely precisely on these properties. The two most common cylindrically polarized modes are the radially and azimuthally polarized modes, described by the annihilation operators \hat{a}_R and \hat{a}_A , respectively. Their annihilation operators are defined as follows,

$$\hat{a}_R = \frac{1}{\sqrt{2}} (\hat{a}_{H10} + \hat{a}_{V01}), \quad \hat{a}_A = \frac{1}{\sqrt{2}} (\hat{a}_{V10} - \hat{a}_{H01}). \quad (4)$$

The entanglement-generating operation is modeled by the squeeze operator

$$\hat{S}(r, \theta) = \exp[r(e^{-i\theta} \hat{a}^2 - e^{i\theta} \hat{a}^{\dagger 2})/2], \quad (5)$$

applied before the beam enters the passive circuit which generates the final cluster state.

In the present work, we propose two schemes to generate two different types of cluster states. A key element in both schemes are, on the one hand, polarizing beam splitters (PBSs), which act as mode separators and combiners and, on

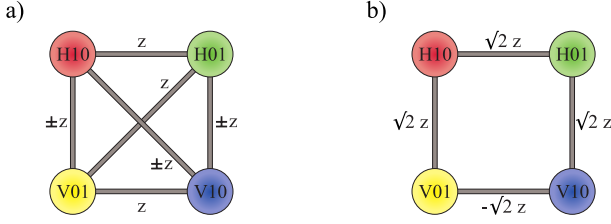


FIG. 2: a) The cluster states generated from scheme 1, and b) from scheme 2. In scheme 1, a quadrature squeezed radially polarized mode is assumed as the input mode. The parameter z is related to the squeezing of the cylindrically polarized mode at the input and, in these plots, quantifies the strength of the entanglement between the different, individually addressable modes.

the other hand, half-wave plates orientated at 22.5° . These rotate the input state by $\hat{a}_{H/V} \mapsto (\hat{a}_H \pm \hat{a}_V)/\sqrt{2}$, thus performing a mode mixing between the different input modes.

The first scheme is illustrated in Fig. 1a). A quadrature squeezed azimuthally (or radially) polarized mode is sent through an array of PBSs and half-wave plates. These are configured in such a way that one gains access to all four basis modes which are spatially separated at the output of the circuit. In Scheme 2, displayed in Fig. 1b), quadrature squeezed azimuthally and radially polarized modes are split into their basis modes. In the next step one pair of orthogonally polarized modes is combined on a PBS and then mixed with a half-wave plate orientated at 22.5° . After the half-wave plate, the modes are separated again at a PBS, therefore allowing one to access all four basis modes in spatially separated arms.

In order to characterize the output states of the proposed schemes, we calculate their adjacency matrices, giving us the full information about any quantum correlations contained in these states. To do so, we make use of the fact that any unitary operation \hat{U} corresponding to a symplectic transformation $\hat{U}^\dagger \hat{\mathbf{x}} \hat{U} = \mathbf{S} \hat{\mathbf{x}}$ changes the covariance matrix \mathbf{C} of a Gaussian state according to

$$\hat{\rho} \mapsto \hat{U} \hat{\rho} \hat{U}^\dagger : \quad \mathbf{C}^\rho \mapsto \mathbf{S} \mathbf{C}^\rho \mathbf{S}^T. \quad (6)$$

For a complete theoretical description of the state, however, we do not only have to consider the co-rotating radially and azimuthally polarized modes, $\hat{a}_{R+} = \hat{a}_R$, $\hat{a}_{A+} = \hat{a}_A$, but also their counter-rotating complements, $\hat{a}_{A-} = (\hat{a}_{V10} + \hat{a}_{H01})/\sqrt{2}$, $\hat{a}_{R-} = (-\hat{a}_{H10} + \hat{a}_{V01})/\sqrt{2}$ (Ref. [34].)

The symplectic matrix for each cluster generation scheme is composed of the matrices of the individual squeezing and passive elements. From the covariance matrix $\mathbf{C}^{\text{out}} = \frac{1}{2} \mathbf{S} \mathbf{S}^T$, one can then extract the adjacency matrix of each scheme according to (3). As a final result for the adjacency matrices describing the cluster graphs for schemes 1 and 2, we obtain

$$\begin{aligned} \mathbf{Z}_1^{A/R} &= i\mathbb{1}_4 + z \tilde{\mathbf{V}}_1^{A/R}, \\ \mathbf{Z}_2 &= 2(z+i)\mathbb{1}_4 + \sqrt{2}z \tilde{\mathbf{V}}_2, \end{aligned} \quad (7)$$

with

$$\tilde{\mathbf{V}}_1^{A/R} = \begin{pmatrix} 1 & \pm 1 & 1 & \pm 1 \\ \pm 1 & 1 & \pm 1 & 1 \\ 1 & \pm 1 & 1 & \pm 1 \\ \pm 1 & 1 & \pm 1 & 1 \end{pmatrix}, \quad \tilde{\mathbf{V}}_2 = \begin{pmatrix} 0 & 0 & 1 & 1 \\ 0 & 0 & 1 & -1 \\ 1 & 1 & 0 & 0 \\ 1 & -1 & 0 & 0 \end{pmatrix}.$$

Here, the first (last) two columns denote the beams with a TEM_{10} (TEM_{01}) spatial profile, while the odd (even) number channels correspond to horizontal (vertical) polarization. The superscripts A and R represent the case for the radial or azimuthal input mode in scheme 1, respectively. The parameter z quantifies the amount of squeezing of the input modes. It is related to the input squeezing in Eq. (5) as $z = (\langle \hat{q} \hat{p}_{\text{in}} \rangle - i \langle \hat{q}_{\text{in}}^2 \rangle + \frac{i}{2}) / 4 \langle \hat{q}_{\text{in}}^2 \rangle$, with $\langle \hat{q}_{\text{in}}^2 \rangle$ and $\langle \hat{q} \hat{p}_{\text{in}} \rangle$ being the (co-)variances of the input mode. For a squeezed input state, these two quantities are given by

$$\begin{aligned} \langle \hat{q}_{\text{in}}^2 \rangle &= \frac{1}{2} [\cosh(2r) - \sinh(2r) \cos \theta], \\ \langle \hat{q} \hat{p}_{\text{in}} \rangle &= -\frac{1}{2} \sinh(2r) \sin \theta. \end{aligned} \quad (8)$$

Here r is the degree of squeezing and θ the squeezing angle. The adjacency matrices clearly show that quantum correlations between the different modes exist and that the output states form a cluster. Especially intriguing is the form of the cluster's graph, showing which modes are directly entangled to each other. The topological structure of these states are displayed in Fig. 2. The cluster state obtained from scheme 1 has the unique feature that all modes are directly linked to each other, corresponding to a so-called fully connected graph. In the case of an azimuthally polarized input beam, it is even *fully symmetric* under permutation of its output modes. The cluster state from scheme 2 displays a box-like structure. Cluster states with this graph topology have already proven their importance for quantum teleportation protocols, both experimentally and theoretically [11, 20].

Our cluster-state generation schemes are distinct from other schemes through the inclusion of the polarization degree of freedom. The cylindrically polarized modes, which form the backbone of the setups, can be manipulated by polarization optics and need only very few interferences. Moreover, the extra polarization degree combined with the spatial degree of freedom constitutes an interesting new information encoding for quantum information processing.

As a proof of principle, we have verified that the cluster state setup suggested in scheme 1 can actually be implemented. The experimental realization is depicted in Fig. 3. A shot-noise limited ORIGAMI laser (Ofive GmbH) emitting 220 fs pulses centered at 1560 nm acts as the light source. The light is injected into an asymmetric Sagnac interferometer [35] and generates an amplitude squeezed linearly polarized Gaussian mode. The key components of the Sagnac loop are a 93:7 beam splitter and a $6.45 \text{ m} \pm 0.02 \text{ m}$ long polarization maintaining single-mode fiber (3M FS-PM-7811) which acts as the nonlinear medium. The Gaussian output mode displays an amplitude squeezing of $-3.3 \text{ dB} \pm 0.1 \text{ dB}$ at a sideband frequency of 10.2 MHz. To realize scheme 1, one

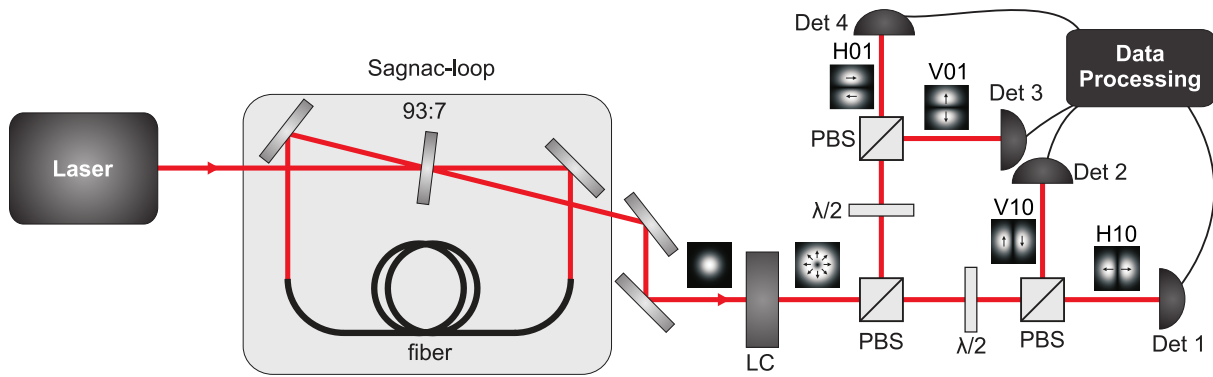


FIG. 3: The experimental setup to generate the cluster state from scheme 1 and measure the amplitude quantum correlations between the different modes. This scheme shows the case where a quadrature squeezed radially polarized beam enters the cluster-state generation circuit. By simply modifying the liquid crystal [LC], also an azimuthally polarized beam can be generated, while the passive circuit remains the same. [polarizing beam splitter (PBS), half-wave plate ($\lambda/2$)]

Correlations	Radial [dB]	Azimuthal [dB]
$\text{Var}\{I_{H01} + I_{H10}\}$	-0.8 (-0.8)	-0.9 (-0.8)
$\text{Var}\{I_{H01} + I_{V10}\}$	-0.8 (-0.8)	-0.9 (-0.8)
$\text{Var}\{I_{V01} + I_{H10}\}$	-0.8 (-0.8)	-0.8 (-0.8)
$\text{Var}\{I_{V01} + I_{V10}\}$	-0.7 (-0.8)	-0.8 (-0.8)
$\text{Var}\{I_{H01} + I_{V01}\}$	-0.8 (-0.8)	-0.9 (-0.8)
$\text{Var}\{I_{V10} + I_{H10}\}$	-0.7 (-0.8)	-0.8 (-0.8)
$\text{Var}\{I_{H01} - I_{H10}\}$	0.0 (0.0)	0.0 (0.0)
$\text{Var}\{I_{H01} - I_{V10}\}$	0.0 (0.0)	0.0 (0.0)
$\text{Var}\{I_{V01} - I_{H10}\}$	0.1 (0.0)	0.0 (0.0)
$\text{Var}\{I_{V01} - I_{V10}\}$	0.1 (0.0)	0.0 (0.0)
$\text{Var}\{I_{H01} - I_{V01}\}$	0.1 (0.0)	0.0 (0.0)
$\text{Var}\{I_{V10} - I_{H10}\}$	0.0 (0.0)	0.0 (0.0)

TABLE I: Amplitude correlation measurements (10.2 MHz sideband) between the different modes of the generated cluster states corresponding to scheme 1 for either the radially or the azimuthally polarized mode as the input mode. The expected theory value is displayed in brackets. The experimental error is ± 0.1 dB in each case.

needs either a quadrature squeezed azimuthally or radially polarized mode. The cylindrically polarized mode is obtained by mode transforming the Gaussian mode with the help of a liquid-crystal polarization converter (ARCOptix) and wave plates [34]. The losses at the device are $17\% \pm 0.5\%$ and we have measured $-1.9\text{ dB} \pm 0.1\text{ dB}$ squeezing in both the radially and azimuthally polarized mode. In the next step, the cylindrically polarized mode goes through a cascade of PBSs and half-wave plates, as indicated in Fig. 1a. The four outputs of the circuit are detected by single detectors with sub-shot noise resolution at a sideband frequency of 10.2 MHz.

The experimental scheme allows one to observe the amplitude quantum correlations present between the different modes. Table I lists all the different correlations and anti-correlations between the different output modes and their ex-

pected theoretical values. We find excellent agreement between the theoretical and experimental results as expected due to the linearity and simplicity of our setup. Stronger correlations can be achieved through higher squeezing of the initial Gaussian mode or by squeezing the individual orthogonal polarization modes as well as the two first-order Hermite Gaussian modes.

It should be noted that in order to fully characterize the system and directly verify the entanglement contained in the cluster, measurements of the conjugate phases and all cross-correlations are also of need. This is however not realizable with the present setup due to the brightness of the resulting beams. However, as a first conceptual proof we may infer from the predicted values for the amplitude correlations the proper behavior of our passive setup.

In conclusion, we have demonstrated that quadrature squeezed cylindrically polarized modes are ideal tools to generate CV cluster states in a compact fashion. The intrinsic entanglement contained within these modes allows for a straightforward generation of cluster states. As each node of the cluster state is a unique mode, these can be easily addressed individually, as needed for measurement-based quantum computations. We have also shown that our approach is versatile and can be exploited to obtain qualitatively different kinds of cluster states, including a fully connected, fully symmetric graph of four optical modes. The protocols proposed here clearly demonstrate that a combination of different polarization states and higher-order spatial modes, realizing a kind of hybrid entanglement of different degrees of freedom, leads to compact and well addressable cluster states. Our system is easily scalable by utilizing higher-order TEM_{nm} modes, and the degree of correlation can be significantly enhanced by squeezing each one of these modes by means of e.g. multi-mode parametric down-conversion. This approach may lead to further enhancement of time-multiplexed schemes which have been used to create very large cluster states [27].

We would like to acknowledge financial support from the

European Union Integrating Project Q-ESSENCE. Peter van Loock wants to acknowledge funding by an Emmy Noether Grant of the DFG.

* These authors contributed equally to this work.

- [1] C. H. Bennett and D. P. DiVincenzo, *Nature* **404**, 247 (2000).
- [2] R. Raussendorf and H. J. Briegel, *Phys. Rev. Lett.* **86**, 5188 (2001).
- [3] R. Raussendorf, D. E. Browne, and H. J. Briegel, *Phys. Rev. A* **68**, 022312 (2003).
- [4] M. A. Nielsen, *Phys. Rev. Lett.* **93**, 040503 (2004).
- [5] P. Walther, K. J. Resch, T. Rudolph, E. Schenck, H. Weinfurter, V. Vedral, M. Aspelmeyer, and A. Zeilinger, *Nature* **434**, 169 (2005).
- [6] M. Van den Nest, A. Miyake, W. Dür, and H. Briegel, *Phys. Rev. Lett.* **97** (2006).
- [7] N. C. Menicucci, P. van Loock, M. Gu, C. Weedbrook, T. C. Ralph, and M. A. Nielsen, *Phys. Rev. Lett.* **97**, 110501 (2006).
- [8] J. Zhang and S. L. Braunstein, *Phys. Rev. A* **73**, 1 (2006).
- [9] X. Su, A. Tan, X. Jia, J. Zhang, C. Xie, and K. Peng, *Phys. Rev. Lett.* **98**, 070502 (2007).
- [10] N. C. Menicucci, S. T. Flammia, H. Zaidi, and O. Pfister, *Phys. Rev. A* **76**, 010302 (2007).
- [11] P. van Loock, C. Weedbrook, and M. Gu, *Phys. Rev. A* **76**, 1 (2007).
- [12] N. C. Menicucci, S. T. Flammia, and O. Pfister, *Phys. Rev. Lett.* **101**, 1 (2008).
- [13] M. Pysher, Y. Miwa, R. Shahrokhshahi, R. Bloomer, and O. Pfister, *Phys. Rev. Lett.* **107**, 030505 (2011).
- [14] N. C. Menicucci, S. T. Flammia, and P. van Loock, *Phys. Rev. A* **83**, 042335 (2011).
- [15] P. Wang, M. Chen, N. C. Menicucci, and O. Pfister, *Phys. Rev. A* **90**, 032325 (2014).
- [16] N. C. Menicucci, *Phys. Rev. Lett.* **112**, 120504 (2014).
- [17] J. Roslund, R. M. de Araújo, S. Jiang, C. Fabre, and N. Treps, *Nature Photon.* **8**, 109 (2013).
- [18] R. N. Alexander and N. C. Menicucci, *Phys. Rev. A* **93**, 062326 (2016).
- [19] U. L. Andersen, J. S. Neergaard-Nielsen, P. van Loock, and A. Furusawa, *Nature Phys.* **11**, 713 (2015).
- [20] M. Yukawa, R. Ukai, P. van Loock, and A. Furusawa, *Phys. Rev. A* **78**, 012301 (2008).
- [21] S. Armstrong, J.-F. Morizur, J. Janousek, B. Hage, N. Treps, P. K. Lam, and H.-A. Bachor, *Nature Commun.* **3**, 1026 (2012).
- [22] O. Pinel, P. Jian, R. de Araújo, J. Feng, B. Chalopin, C. Fabre, and N. Treps, *Phys. Rev. Lett.* **108**, 22 (2012).
- [23] N. C. Menicucci, X. Ma, and T. C. Ralph, *Phys. Rev. Lett.* **104**, 250503 (2010).
- [24] N. C. Menicucci, *Phys. Rev. A* **83**, 062314 (2011).
- [25] M. Chen, N. C. Menicucci, and O. Pfister, *Phys. Rev. Lett.* **112**, 120505 (2014).
- [26] S. Yokoyama, R. Ukai, S. C. Armstrong, C. Sornphiphatphong, T. Kaji, S. Suzuki, J.-I. Yoshikawa, H. Yonezawa, N. C. Menicucci, and A. Furusawa, *Nature Photon.* **7**, 982 (2013).
- [27] J.-I. Yoshikawa, S. Yokoyama, T. Kaji, C. Sornphiphatphong, Y. Shiozawa, K. Makino, and A. Furusawa, *Appl. Phys. Lett. Photon.* **1**, 060801 (2016).
- [28] C. Gabriel, A. Aiello, W. Zhong, T. G. Euser, N. Y. Joly, P. Banzer, M. Förtsch, D. Elser, U. L. Andersen, C. Marquardt, et al., *Phys. Rev. Lett.* **106**, 1 (2011).
- [29] A. Aiello, F. Töppel, C. Marquardt, E. Giacobino, and G. Leuchs, *New J. Phys.* **17**, 043024 (2015).
- [30] B. C. dos Santos, K. Dechoum, and A. Z. Khoury, *Phys. Rev. Lett.* **103** (2009).
- [31] M. Lassen, G. Leuchs, and U. L. Andersen, *Phys. Rev. Lett.* **102**, 163602 (2009).
- [32] T. G. Euser, M. Schmidt, N. Y. Joly, and C. Gabriel, *J. Opt. Soc. A. B* **28**, 193 (2011).
- [33] H. J. Briegel and R. Raussendorf, *Phys. Rev. Lett.* **86**, 910 (2001).
- [34] A. Holleczek, A. Aiello, C. Gabriel, C. Marquardt, and G. Leuchs, *Opt. Express* **19**, 9714 (2011).
- [35] S. Schmitt, J. Ficker, M. Wolff, F. König, A. Sizmann, and G. Leuchs, *Phys. Rev. Lett.* **81**, 2446 (1998).